pISSN:2093-274x eISSN:2093-2480
DOI:10.5139/IJASS.2010. 11. 1.001

Numerical Simulation of Rotor-Fuselage Aerodynamic Interaction Using an Unstructured Overset Mesh Technique

Bum Seok Lee*, Mun Seung Jung* and Oh Joon Kwon**
Department of Aerospace Engineering,
Korea Advanced Institute of Science and Technology, Daejeon, 305-701, Korea

Hee Jung Kang***
Rotorcraft Department, Rotorcraft Development Division,
Korea Aerospace Research Institute, Daejeon, 305-333, Korea

Abstract

Numerical simulation of unsteady flows around helicopters was conducted to investigate the aerodynamic interaction of main rotor and other components such as fuselage and tail rotor. For this purpose, a three-dimensional inviscid flow solver has been developed based on unstructured meshes. An overset mesh technique was used to describe the relative motion between the main rotor, and other components. As the application of the present method, calculations were made for the rotor-fuselage aerodynamic interaction of the ROBIN (ROtor Body INteraction) configuration and for a complete UH-60 helicopter configuration consisted of main rotor, fuselage, and tail rotor. Comparison of the computational results was made with measured time-averaged and instantaneous fuselage surface pressure distributions for the ROBIN configuration and thrust distribution and available experimental data for the UH-60 configuration. It is demonstrated that the present method is efficient and robust for the simulation of complete rotorcraft configurations.

Key Word : Rotor fuselage interaction, Unstructured mesh, Overset mesh technique, ROBIN, UH-60

Introduction

Prediction of unsteady flow fields around helicopters is one of the most difficult problems in modern CFD. The tip vortex interacting with rotor blades causes Blade-Vortex Interaction (BVI) which generates highly directional impulsive noise and sudden change in the blade aerodynamic loading. The aerodynamic interaction between the rotor wake and the fuselage results in unsteady loading on the fuselage, and causes a fuselage vibration problem. These aerodynamic interactions significantly affect on the performance of helicopters and can cause structural damage. Therefore, precise understand of the aerodynamic interaction between rotor, fuselage, and other components is needed. However, the existence of fuselage underneath the rotor amplifies the complexity of analysis, and the unsteadiness of the rotor wake and the asymmetric nature of the rotor disk loading make it difficult to predict the flow field around the full helicopter configuration.

Several research works have been conducted previously to calculate the complicated unsteady flow fields around helicopters involving mutual aerodynamic interaction between the rotor and the fuselage. As the traditional way, lifting line/free-wake methods coupled with potential theory have been used to model the rotor blades and the fuselage [1- 3]. These methods are computationally inexpensive and provide fundamental understanding of the rotor fuselage phenomena, but are limited to inviscid flows.

Owing to the development of high performance computers, analysis of rotor fuselage interaction became possible with the Euler or Navier-Stokes methods modeling with a simplified modeling of rotor such as the actuator disc[4, 5].

* Graduate Student
** Professor
E-mail : ojkwon@kaist.ac.kr
Tel : +82-42-350-3720 Fax : +82-42-350-3710
*** Researcher

These methods provide reasonable time-averaged/time accurate solutions, but because of the simplified representation of the rotor, it is difficult to capture the precise influence of the rotor wake on the fuselage and the unsteady flow features such as the tip-vortex generation, or blade-vortex interaction.

As an alternative to above-mentioned methods, a method that describes the relative motion between the rotor and the fuselage directly has been developed using either sliding mesh or structured overset mesh technique [6-8]. Through these methods, it became possible to model the both fuselage and rotor with high resolution Euler/Navier-Stokes methods. However, because of the regularity required in the grid point distribution, the overset method based on structured grids is difficult to enhance the local resolution of the solution by mesh adaptation. Also, it is known that the sliding mesh method is not robust when mesh deformation becomes severe due to large blade motion or deflection.

Recently, to overcome these limitations, the methods based on unstructured overset mesh have been widely used by many researchers, because unstructured mesh methods have an advantage of handling complex geometry and can easily improve the solution accuracy by refining cells locally as required [9-11].

In the present study, a numerical method has been developed for the simulation of inviscid unsteady flows around a complete rotorcraft configuration based on unstructured meshes. Even though it is also possible to simulate unsteady flowfield with viscous method, the calculation is still expensive compared to inviscid method. To describe the relative motion between the main rotor, and other components, an overset mesh technique was adopted. To enhance the spatial accuracy of the solution, a quasi-unsteady solution-adaptive mesh refinement technique was applied.

For the application of the present method, calculations were made for the rotor-fuselage interaction of the ROBIN configuration. The results were compared with experimental data. As the second application, the mutual interference between main rotor, fuselage, and tail rotor of a complete UH-60 configuration was investigated. The flowfield and the airloads on the rotor were examined. From the results, the characteristics of the rotor-fuselage interaction and the mutual interference effect on overall flowfield around a helicopter were demonstrated.

Numerical Method

2.1 Spatial Discretization and Time Integration

The equations governing three-dimensional, inviscid, unsteady, compressible flows are the Euler equations, which can be recast in an integral form for a bounded domain V with boundary ∂V ;

$$\frac{\partial}{\partial t}\iiint_V Q\, dV + \iint_{\partial V} F(Q)\cdot \vec{n}\, dS = 0 \qquad (1)$$

where $Q=[\rho, \rho u, \rho v, \rho w, e_0]$ is the solution vector of the conservative variables for the mass, momentum and energy equations. The governing equations were discretized using a vertex-centered finite-volume method. The flow domain was divided into a finite number of control volumes surrounding each vertex, which are made of a non-overlapping median-dual cell whose boundary surfaces are defined by the cell centroid, face centroid, and mid-point of the edge. The inviscid flux term, $F(Q)$, was computed using Roe' s flux-difference splitting scheme [12]. The flow variables at each dual face were computed by using a linear reconstruction technique to achieve second-order spatial accuracy. In this approach, the face value of the primitive variables was calculated from those at the dual face using the averaged solution gradient of each control volume obtained from a least-square procedure.

An implicit time integration algorithm based on a linearized second-order Euler backward differencing was used to advance the solution in time. The linear system of equations was solved at each time step using a point Gauss-Seidel method.

2.2 Boundary Condition

On the solid surface of the fuselage and the rotor blades, the flow tangency condition was imposed. The density and the pressure on the solid surface were obtained by extrapolating from the interior domain. At the far-field boundary, the characteristic boundary condition with Riemann invariants was used.

2.3 Unstructured Overset Mesh Technique

To handle multiple bodies in relative motion effectively, an overset mesh scheme was adopted [13]. For the overset mesh method, a search procedure is needed for the identification of donor cells that contain the verticies from the opposite overlapping mesh block. For unstructured meshes, the search should be performed for all nodes of all mesh blocks, because the nodes and the cells are randomly distributed. To overcome the large computational overhead involved in this search process, a fast and robust neighbor-to-neighbor search technique was implemented by utilizing the property of the linear shape functions [14]. Under parallel computing environment, the search may

develop across the subdomain block boundary, and the amount of data information assigned to each processor may change at each iteration. To handle this varying amount of calculation load efficiently, a new data structure for parallel distributed memory machine was implemented.

Once the search process is completed, the information is used for clarifying the node type and for determining the weighting factors necessary for the interpolation. In the present overset mesh method, a distance-to-wall technique [15] was implemented for grouping active nodes and non-active nodes. Hole cutting for determining cell types as either active, interpolation, or non-active was made based on the number of active nodes assigned to each tetrahedral cell. Then interpolation and transfer of the flow variables were made between adjacent mesh blocks. In order to reduce the error involved in the interpolation, both the cell containing the interpolation receiver and also the neighboring cells enclosing that cell were considered.

2.4 Mesh Adaptation

To reduce the numerical dissipation and to enhance the spatial accuracy of the solution, a solution-adaptive mesh adaptation procedure was applied. In the present study, a quasi-unsteady mesh refinement technique was adopted to avoid excessive computational time required by dynamic mesh adaptation applied in a fully unsteady manner.

In this approach, as the blade rotates, cells having high vorticity are tagged at every time step. Once the rotor completes one period of rotation, the calculation is paused and the tagged cells are divided. Then the refined mesh is repartitioned for load balancing and the calculation resumes. The tagged cells are divided by adding new nodes in the middle of six edges of each tetrahedral cell. Buffer cells are also used to preserve the connectivity between the divided and surrounding cells.

The mesh adaptation was performed for each individual mesh block, independent to other blocks.

2.5 Rotor Trim

For rotors in forward flight, to retain the calculated thrust to the experimental value and to eliminate the rotor aerodynamic moment, a rotor trim procedure was adopted. The thrust and moment coefficients can be expressed as a function of the collective and cyclic pitch angles. Then the equilibrium state was obtained by adjusting the trim angles iteratively using a Newton-Raphson method.

2.6 Parallel Computation

In order to reduce the large computational time to handle a large number of cells, a parallel computational algorithm based on a domain decomposition strategy was adopted. The load balancing between processors was achieved by partitioning the global computational domain into local subdomains using the MeTiS libraries. The Message Passing Interface was used to transfer the flow variables across the subdomain boundary. This load balancing was made for each sub-block mesh, and thus was not strictly enforced for the global computational domain. All calculations were made on Linux-based PC clusters having 2.5G Hz Intel Core 2 Quad CPU.

Result and Discussion

Initially, calculation was made for the ROBIN rotor-fuselage configuration to validate the capability of the present method for accurately predicting induced downwash by the main rotor and the rotor-fuselage aerodynamic interference phenomena. Then the present method was applied to a complete configuration of UH-60 helicopter composed of main rotor, tail rotor, and fuselage.

3.1 ROBIN Configuration

ROBIN (ROtor Body INteraction) [16] is a generic rotor-fuselage configuration consisted of a super ellipse-shaped fuselage and four blades. The blade has a rectangular platform shape with an NACA 0012 airfoil section, and is linearly twisted by -8 degrees from blade root to tip. The aspect ratio of the blade is 12.98, and the root cut-out is 0.24R. The operating blade tip Mach number is 0.523. Among the various experimental conditions, three advance ratios of μ=0.012, 0.15, and 0.23 that have the same time-averaged thrust coefficient C_T=0.0064 were simulated.

In Fig. 1, the computational overset mesh consisted of five mesh blocks is presented. The main block covers the complete computational domain and the fuselage. The four sub-blocks cover each of the four rotor blades. The mesh was constructed with 284,623, 255,472, 255,472 vertices for the main block for each advance ratio of μ=0.012, 0.15, and 0.23, respectively, and 143,654, 143,654, 143,654 vertices for the sub-block for each advance ratio. After one level of mesh adaptation, the number of vertices increased to 1,241,460, 1,291,092, 1,280,972 for the main block and 227,457, 217,064, 191,346 for each

Table 1. Comparison of blade collective and cyclic pitch angles for ROBIN configuration

	Experiment				Simulation			
μ	C_T	A_0	A_1	B_1	C_T	A_0	A_1	B_1
0.012	0.0063	11.8	−0.1	0.2	0.0063	8.8	−0.1	0.2
0.15	0.0064	10.3	−2.7	2.4	0.0064	6.64	−2.356	2.288
0.23	0.0064	10.4	−0.4	3.8	0.0064	6.523	−1.906	3.434

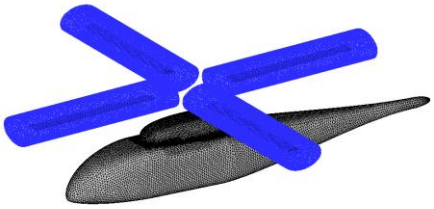

Fig. 1. Computational overset mesh blocks for ROBIN configuration

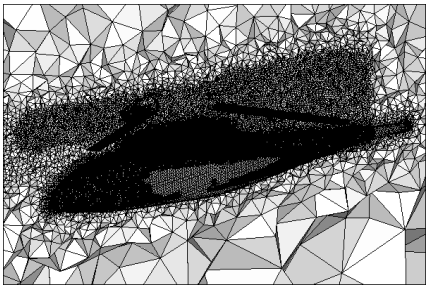

Fig. 2. Computational mesh for the ROBIN configuration after mesh adaptation at μ = 0.15

sub−block. In Fig. 2, the computational mesh distribution after mesh adaptation for μ=0.15 is presented at the fuselage symmetric plane. It is shown that small cells are distributed around the blades and the fuselage where the inference between the two components becomes most severe.

For the accurate simulation, the blade control angle setting was adjusted until the calculated thrust matched to that of the experiment. The trim of rotor was conducted with the coarse mesh. The rotor was advanced by 0.25 degrees at each time step. In the case of the advance ratio of μ=0.012, since the advance ratio is very small, the rotor trim was performed only for the collective pitch angle, and the longitudinal and lateral cyclic pitch angles were used as provided from the experiment. In table 1, comparison of the experimentally measured control angles and the The converged solution was achieved after 18, 36, 33 revolutions for each advance ratio μ =0.012, 0.15, and 0.23, respectively.

Figs. 3 and 4 show the comparison of theunsteady pressure coefficient with theexperimental data. The results are represented as the modified pressure coefficient that is non−dimensionalised by the rotor tip speed and multiplied by 100. It is also noticed that the experimental unsteady pressure data presented in this paper were shifted in phase by 252 degrees[17] from the original data to correct the phase delay occurred in the experiment.

In Fig. 3, unsteady pressure variations along the top center of the fuselage are compared with the experiment at four selected surface points. Although there is small deviation in the phase from the experiment, the overall results are in good agreement with the experiment for both magnitude and phase.

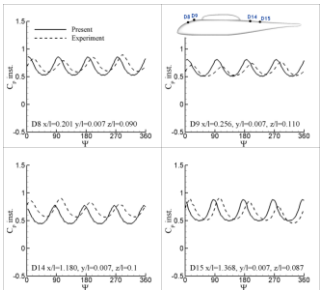

(a) μ=0.012, C_T=0.0063

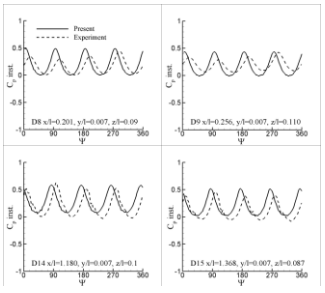

(b) μ=0.15, C_T=0.0064

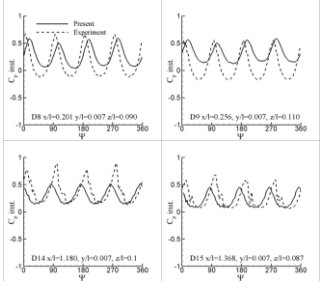

(c) μ=0.23, C_T=0.0064

Fig. 3. Unsteady pressure variation along fuselage top center

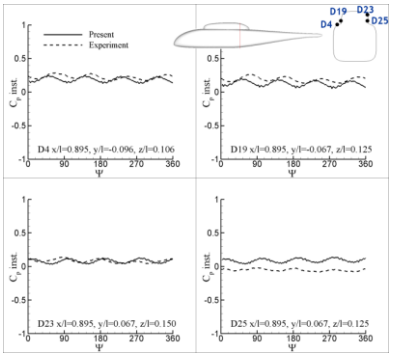

(a) μ=0.012, C_T=0.0063

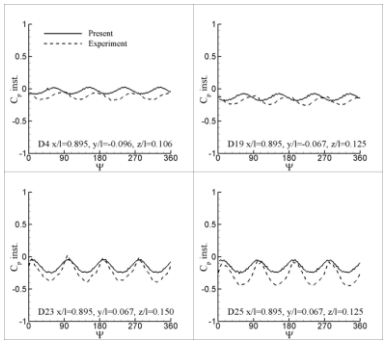

(b) μ=0.15, C_T=0.0064

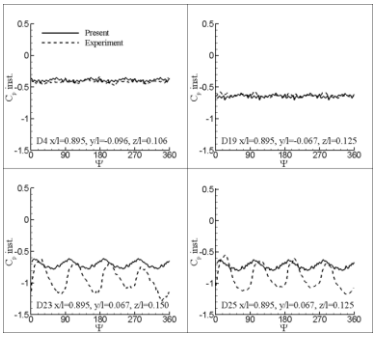

(c) μ=0.23, C_T=0.0064

Fig. 4. Unsteady pressure variation around fuselage at x/l=0.9

In Fig. 4, unsteady pressure variations around the fuselage at the streamwise station x/l=0.9 are compared with the experiment at four selected points; two at the advancing side of the fuselage, D23 and D25, and the other two at the retreating side, D4 and D19. It is shown that the results compare reasonably well with the experiment, even though the phase difference still exists between the two results.

The time-averaged pressure distributions around the fuselage at two selected streamwise locations are compared with the experiment in Fig. 5. It is shown that good comparison is made at X/l=0.35 located ahead of the pylon. At the location downstream of the pylon, X/l=1.17, the overall agreement is fair, and some deviation is observed, particularly at negative z-locations. This is presumably due to the fact that these points are under the fuselage and are affected by the structure supporting the fuselage in the experiment, which is not modeled in the present simulation.

In Fig. 6, the instantaneous vorticity contours are presented at the fuselage symmetric plane. It is shown that the fuselage is completely submersed inside the rotor wake, and the tip vortex directly impinges to the fuselage at advance ratio of μ=0.012. However, as the advance ratio increases, rotor wake becomes skewed further such that only the rear part of ROBIN fuselage is affected. At the advance ratio of μ=0.15, the rear part of pylon and tail boom of fuselage is affected by the wake, but at μ=0.23, the direct impingement of wake is not observed.

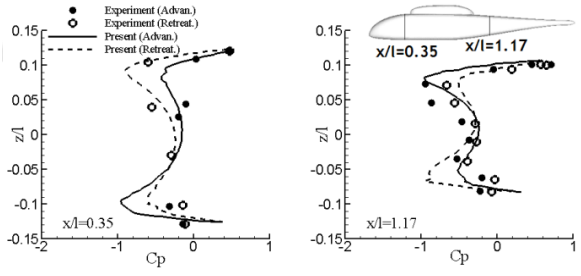

(a) μ=0.012, C_T=0.0063

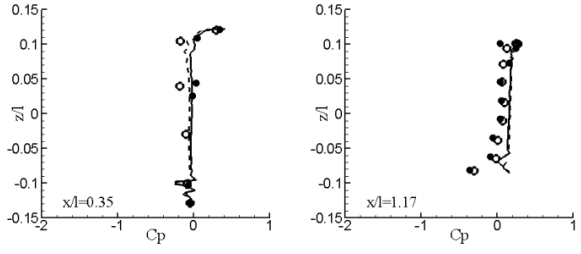

(b) μ=0.15, C_T=0.0064

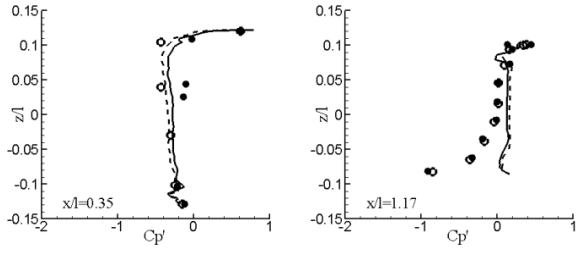

(c) μ=0.23, C_T=0.0064

Fig. 5. Time-averaged pressure distribution around fuselage at two selected streamwise stations

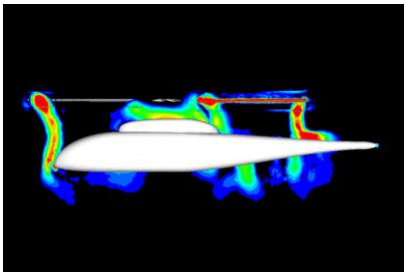

(a) μ=0.012, C_T=0.0063

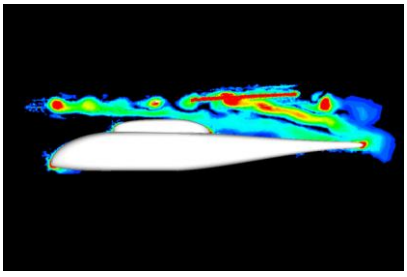

(b) μ=0.15, C_T=0.0064

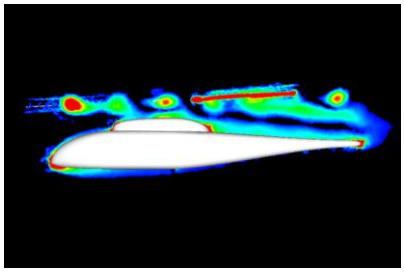

(c) μ=0.23, C_T=0.0064

Fig. 6. Instantaneous vorticity contours at the fuselage symmetric plane for blades aligned along Ψ = 0 °

3.2 Complete UH-60 Configuration

As the second validation, the mutual interaction of main rotor, fuselage, and tail rotor was simulated for a complete UH−60 helicopter configuration. The main rotor is consisted of four blades that are made of SC−1095 and SC−1094 airfoil sections, and have an aspect ratio of 15.51 [18]. The blade of the tail rotor has an aspect ratio of 3.1, and the gear ratio of the tail rotor to the main rotor is 4.62 [19]. For the simplicity of the calculation, the engine casing and the landing gear were not modeled. The calculation was made for a hovering flight condition at a blade tip Mach number of 0.65 and a collective pitch angle of 9.2° with C_T/σ=0.085.

In this calculation, a simplified trim was made such that the torque produced by the main rotor is compensated by the tail rotor. For this purpose, the collective pitch angle of the tail rotor blade was adjusted until the main rotor torque C_q obtained experimentally [20], 6.7732X10^{-4}, was cancelled by

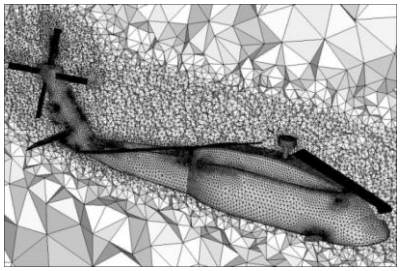

Fig. 7. Computational mesh for UH 60 configuration

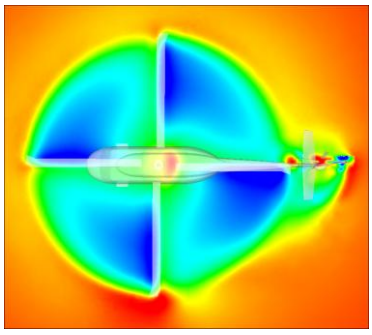

Fig. 8. Inflow contours at one chord length above rotor disk plane

the thrust of the tail rotor multiplied by the moment arm from the axis of the main rotor to the tail rotor. The resultant collective pitch angle of the tail rotor blade was 18.8° , which provided an anti−torque C_q of 6.7372X10^{-4}.

Fig. 7 shows the mesh distribution on the surface of the UH− 60 configuration and at the fuselage symmetric cutting plane. The computational overset mesh contained 504,488, 679,940, and 110,040 vertices in each mesh block for fuselage, main rotor, and tail rotor, respectively. It is shown that fine cells are distributed around the main rotor, tail rotor, and fuselage to capture the wake and the aerodynamic interaction phenomena more accurately. The total number of cells used was 6,902,466.

In Fig. 8, the downwash inflow contours at one chord length above the rotor disk plane is presented. It shows that the contours are slightly distorted near Ψ = 0 ° , showing higher inflow in this region. This is because strong sidewise flow is pumped by the tail rotor, which sucks in a substantial amount of downwash flow from the main rotor. As a result, the magnitude of downwash near the tail rotor along the rotor azimuth angle Ψ = 0° increased. In Fig. 9, the downwash distribution along Ψ = 0° at one chord length above the rotor disk plane is presented. The result is also compared with that of the rotor−fuselage configuration without the tail rotor. The figure shows that higher

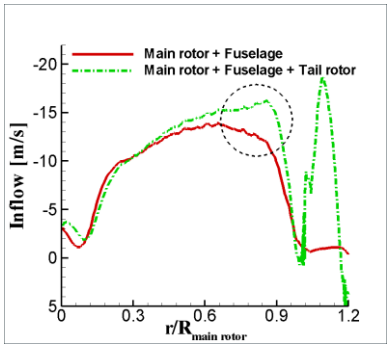

Fig. 9. Inflow distribution along $\Psi = 0°$ at one chord length above rotor disk plane

downwash is obtained near the tip of the main rotor blade and slightly off the rotor disk plane due to the interaction with the tail rotor, which subsequently reduces the effective angle of attack for the main rotor blade in this region, compared to the case without the tail rotor.

In Fig. 10, spanwise sectional thrust distributions of the main rotor blade at four azimuth angles are presented, and the results are compared with those of an isolated rotor and the rotor-fuselage configuration. It is shown that allThree calculatedresults are similar to each other, and compare well with the experiment obtained for the rotor-alone configuration. However, at $\Psi = 0°$, the thrust loading for theconfiguration with the tail rotor is substantially lower

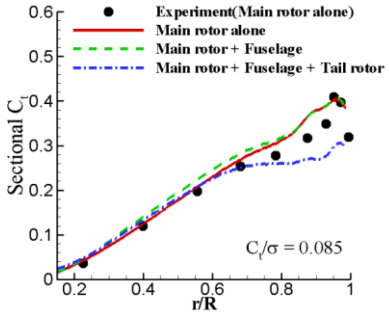

(a) $\Psi = 0°$

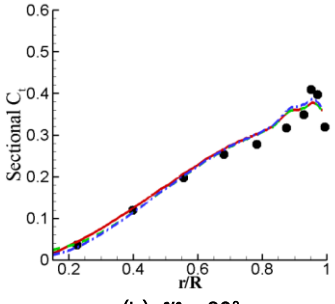

(b) $\Psi = 90°$

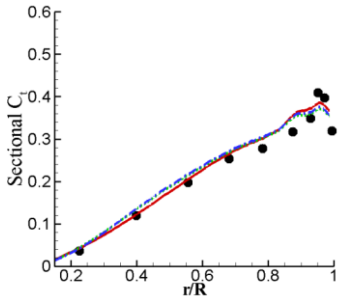

(c) $\Psi = 180°$

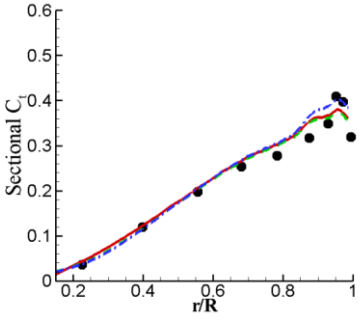

(d) $\Psi = 270°$

Fig. 10. Spanwise sectional thrust loading distribution on main rotor blade

than the other two cases near the blade tip region. This confirms that higher induced downwash exists in the region near the tail rotor, which reduces the effective angle of attack and thus the blade loading.

In Fig. 11, the sectional thrust contours are presented for one revolution of the main rotor. It is shown that a significant distortion of blade loading exists for the rotor azimuth angle between 320° and 15°, due to the interference with the tail rotor as described above, which could be a potential source of blade vibration.

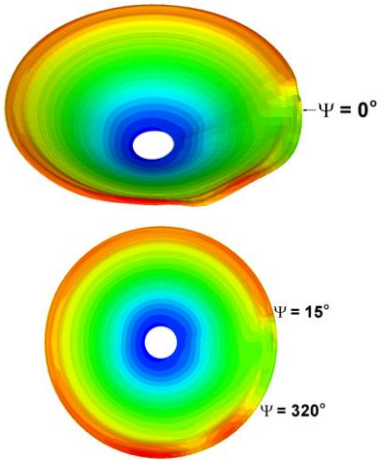

Fig. 11. Sectional thrust contours for one revolution of main rotor

Conclusion

Numerical simulations of unsteady flows around helicopters were conducted to investigate the aerodynamic interaction between the main rotor and other components. For this purpose, a vertex-centered finite-volume flow solver based on unstructured meshes has been developed. An overset mesh technique was used to describe the relative motion between the main rotor and other components, and a quasi-unsteady solution-adaptive mesh technique is used to enhance the spatial accuracy of the solution. As the application of the present method, calculations were made for the rotor-fuselage interaction of the ROBIN configuration and for a complete UH-60 helicopter configuration. From the results, it was found that significant mutual interference exists between the main rotor and other components, and this interaction affects unsteady flow characteristics and the aerodynamic loads of helicopters. It was also demonstrated that the present method is efficient and robust for simulating unsteady rotor-fuselage interaction.

Acknowledgments

This study has been supported by the KARI under the KHP Dual-Use Component Development Program funded by the MOCIE.

References

1. D. N. Marvris, N. M. Kmerath, and H. M. McMahon, "Prediction of Aerodynamic Rotor-Airframe Interactions in Forward Flight", *Journal of the American Helicopter Society*, Vol. 34, No. 4, pp. 37-46, 1989.

2. P. E. Lorber, and T.A. Egolf, "An Unsteady Helicopter Rotor-Fuselage Aerodynamic Interaction Analysis", *Journal of the American Helicopter Society*, Vol. 35, No. 3, pp. 32-42, 1990.

3. D. A. Wachspress, T. R. Quackenbush, and A.H. Boschitsch, "Rotorcraft Interactional Aerodynamics with Fast Vortex/Fast Panel Methods", *Journal of the American Helicopter Society*, Vol. 48, No. 4, October 2003.

4. M. S. Chaffin, and J. D. Berry, "Helicopter Fuselage Aerodynamics Under a Rotor by Navier-Stokes Simulation", *Journal of the American Helicopter Society,* Vol. 42, No. 3, pp. 235-243, 1997.

5. D. D. Boyd, and R. W. Barnwell, "A Computational Model for Rotor-Fuselage Interactional Aerodynamics", *AIAA Paper 2000-0256,* AIAA 38th Aerospace Sciences Meeting & Exhibit, Reno NV, January 10-13, 2000.

6. Y. M. Park, H. J. Nam, and O. J. Kwon, "Simulation of Unsteady Rotor-Fuselage Interactions Using Unstructured Adaptive Meshes", *Journal of the American Helicopter Society,* Vol. 51, No. 2, pp. 141-149, 2006.

7. N. S. Hariharan, and L. N. Sankar, "Numerical Simulation of the Fuselage-Rotor Interaction Phenomenon", *AIAA Paper 96-0672*, 1996.

8. R. Stangl, and S. Wagner, "Euler Simulation of a Helicopter Configuration in Forward Flight using a Chimera Technique", *Proceedings of the 52nd Annual Forum of the American Helicopter Society*, pp. 453-462, 1996.

9. M. Dindar, A. Z. Lemnios, M. S. Shephard, and J. E. Flaherty, "An Adaptive Solution Procedure for Rotorcraft Aerodynamics", *AIAA Paper 98-2417*, 1998.

10. H. J. Kang, and O. J. Kwon, "Effect of Wake Adaptation on Rotor Hover Simulations Using Unstructured Meshes", *Journal of the Aircraft,* Vol. 38, No. 5, pp. 868-877, 2001.

11. H. J. Kang, and O. J. Kwon, "Unstructured Mesh Navier-Stokes Calculations of the Flowfield of a Helicopter Rotor in Hover", *Journal of the American Helicopter Society*, Vol. 47, No. 2, pp. 90-99, 2002.

12. P. L. Roe, "Approximate Riemann Solvers, Parameter Vectors and Difference", *Journal of Computational Physics*, Vol.43, No. 2, pp. 357-372, 1981.

13. M. S. Jung and O. J. Kwon, "A Parallel Unstructured Hybrid Overset Mesh Technique for Unsteady Viscous Flow Simulations", Presented at the International conference on Parallel Computational Fluid Dynamics, *ParCFD 2007-024*, 2007.

14. M. S. Jung and O. J. Kwon, "A Conservative Overset Mesh Scheme via Intergrid Boundary Reconnection on Unstructured Meshes", *AIAA Paper 2009-3536*, San Antonio, TX, June 2009.

15. K. Nakahashi, F. Togashi, and D. Sharov, "Intergrid-Boundary Definition Method for Overset Unstructured Grid Approach", *AIAA Journal*, Vol. 38, No. 11, pp. 2077-2084, 2000.

16. E. M. Raymond and S. A. Gorton, "Steady and Periodic Pressure Measurements on a Generic Helicopter Fuselage Model in the Presence of a Rotor", *NASA TM 2000-210286*, 2000.

17. A. R. Kenyon and R. E. Brown., "Wake Dynamics and Rotor Fuselage Aerodynamic Interactions", *Presented at the AHS 63rd Annual Forum*, Virginia Beach, May 1-3, 2007.

18. W. G. Bousman, "Aerodynamic Characteristics of SC1095 and SC 1094 R8 Airfoils", *NASA/TP-2003-212265*, 2003.

19. K. B. Hilbert, "A Mathematical Model of the UH-60 Helicopter", *NASA TM 85890*, 1984.

20. B. E. Wake and J. D. Beader, "Evaluation of a Navier-Stokes Analysis Method for Hover Performance Prediction", *Journal of the American Helicopter Society*, Vol. 41, No. 1, pp. 7-17, 1996.